Study of Composition and Optical Properties of Chemically Deposited Pd-xSb$_2$S$_3$ Thin Films

Patrick Akata Nwofe

Department of Industrial Physics, Ebonyi State University, Abakaliki, P.M.B 053, Nigeria

ABSTRACT

The study reports on the effects of different concentration of palladium impurities on the compositional and optical properties of Palladium Doped Antimony Sulphide (Pd-xSb$_2$S$_3$) thin films grown by the chemical bath deposition method. The films were grown at room temperature and other deposition conditions such as the bath temperature, pH, complexing agents were kept constant. The concentration of the dopants were varied between 0.1 M to 0.3 M. The films were annealed at an annealing temperature of 200 °C for 1 hour. The films were characterised using the Rutherford Back Scattering (RBS) techniques and optical spectroscopy (transmittance versus wavelength, absorbance versus wavelength) to investigate the composition, and optical constants (optical absorption coefficient, energy band gap, and extinction coefficient) respectively. X-ray diffractometry and Scanning electron microscopy were also used to investigate the structural and morphological properties of the layers. The results show that the transmittances of the doped layers were higher compared to the as-deposited layers. The energy band gap was direct, and were found to be decreased for the doped layers, compared to the as-grown films. The values of the energy band gap were typically ≤ 2.30 eV for the former and 2.48 eV for the latter. These values strongly suggest the use of these films in optoelectronic applications especially in solar cell devices.

INTRODUCTION

In recent times, the potentials of antimony sulphide (Sb$_2$S$_3$) for use in various optoelectronic and solar thermal devices including solar cell applications have been widely established in the literature [1-4]. Antimony Sulphide is a direct band gap semiconductor material that has been under investigation for use in various device designs over the years and most recently, for application in photovoltaic solar cell devices. For instance, in photovoltaic applications, Sb$_2$S$_3$ has been used as the p-type absorber layers in making heterojunction solar cell devices [5] with improved solar conversion efficiency. The use of antimony sulphide thin film for applications in other optoelectronic devices, medicinal use, luminescence materials, and in various industrial uses have been widely reported in the literature [6-14]. Reports by different research groups indicate that antimony sulphide thin films can be grown using variety of different thin film technology including; spray pyrolysis [15-16], pulsed laser ablation deposition technique [17] laser assisted-chemical bath deposition [18], Chemical vapour deposition method [2], spin technique [4], chemical bath deposition technique [6-7], pulsed electro-deposition technique [19], two-stage process [20], rapid thermal process

* Corresponding Author Email: patricknwofe@gmail.com

[21], hydrothermal deposition method [22], sulphidisation method [23], thermal evaporation [24-25], successive ionic layer and reaction (SILAR) technique [26], photochemical deposition method [27], etc.

It is a common knowledge that chemical bath deposition method is a more universally used technique due to the fact that the method offers high quality thin films at low temperature, suitable for depositing large area semiconductor thin films, and has proved to be the simplest and the most economical since the equipment used for deposition are very common and easily affordable. It is understood that thin film deposition on a substrate can be achieved by either or all of the two steps of nucleation and particle growth. In general, for thin films grown by the solution growth technique, the process of nucleation and film growth are mostly due to an inter-play of other processes which includes; simple-ion cluster mechanism, simple hydroxide cluster mechanism, complex ion-by-ion decomposition mechanism, and the complex-cluster decomposition mechanism. The simple ion process could diffuse to the substrate to initiate nucleation and the nucleated layers then grow by adsorption of ions in the solution and or nucleation of new crystals. The films formed by the crystals are generally held together by weak forces (Van der Waals forces). Thus, the chemical bath deposition process mostly employs a controlled chemical reaction to achieve thin film deposition by precipitation of the desired compound.

According to the literature [26-29], the intrinsic properties of Sb$_2$S$_3$ thin films has been modified by introducing different impurities in order increase the versatility of Sb$_2$S$_3$–based thin films in different applications. The use of palladium impurities to optimise the properties of Sb$_2$S$_3$ thin films is relatively rare in the literature hence to the best of our knowledge, this report is novel in engineering the properties of Sb$_2$S$_3$ thin films for enhanced device applications. In the present investigation, the aim of the study is to grow thin films of Sb$_2$S$_3$, dope the layers with different concentrations of the dopants, and to characterise the layers using compositional and optical spectroscopy to investigate the composition and the optical constants respectively. This report is a fundamental step toward exploring new pathways for utilization of Sb$_2$S$_3$-based thin films in different device designs.

MATERIALS AND METHODS

Substrate cleaning plays a fundamental role in thin film deposition. The glass slides of dimensions 75 mm by 25 mm by 1mm, were purchased from local suppliers. Prior to the deposition, the glass substrates were cleaned first by a mild detergent solution, then degreased with acetone, and further etched with 5% of hydrochloric acid (HCl) for 60 minutes. Finally, the glass slides were cleaned ultrasonically by double distilled water and then dried in air. All the source chemicals used for the deposition of Sb$_2$S$_3$ thin films were analytical grade, and were obtained from Sigma Aldrich UK through local suppliers and employed directly without further purification. The source of the antimony ions and sulphide ions were antimony trichloride (Sb$_2$Cl$_3$) and sodium thiosulphate (Na$_2$SO$_3$) respectively.

A 4g of antimony trichloride with the desired amount of acetone was prepared and included in a clean beaker and sealed. A 31 g of sodium thiosulphate powder was dissolved in 125 ml of water and stirred for 15 minutes. The reaction bath contained a 20 ml each of the cation source Sb+, and anion source S-, and 10 ml of the complexing agent, and then stirred for 10 minutes using a magnetic stirrer. The temperature of the reaction bath was maintained at 298 K and the rotational speed of the stirrer was fixed at 50 revolutions per minute. The pH of the solution was found to be acidic, typically 5.0. The solution was then distributed into 2 separate beakers with one kept as control, and in the other, a 10 ml of the different concentrations of the dopant were included separately and carefully labelled. The glass substrates were held vertically using a synthetic foam and deposition was allowed to take place for 1 hour. The films were then removed carefully at the end of the deposition time, and washed with distilled water, and then dried.

The film thickness was measured using standard procedure in the current literature as reported by different authors [6-8], hence the film thickness was measured using the gravimetric method or double weight method. The film thickness were in the range 185 nm for the as-deposited layers and between 205 nm to 215 nm for the doped layers. The transmittance and absorbance versus wavelength measurements were done using a Unico –UV-2102 PC spectrophotometer operated at normal incident of light in the wavelength range of 300 nm to 1000 nm.

RESULTS AND DISCUSSION

Fig. 1 show the transmittance versus wavelength plots for the as-grown layers and layers doped at the respective concentrations of the palladium impurities. The transmittance exhibited a concentration dependent behaviour in that the transmittances were higher for films grown at concentrations ≤ 0.3 M and decreased by almost 50% for the as-grown films. This behaviour was attributed to the increase in the film thicknesses at the higher concentrations of the palladium impurities. Such increase can cause an increase in the crystallites sizes in the films grown at the higher concentrations. The increased crystallites size as they tend to approach the bulk crystalline Sb_2S_3 could lead to larger unfilled inter-granular volume so that the absorption per unit thickness is reduced in the films, hence causing the observed phenomena.

Fig. 1 also reveals that a blue shift effect is induced by the introduction of the palladium impurities on the transmittance spectra. This observation could be attributed to the effect quantum confinement as a result of the reduced particle dimension as the dopants tend to blend with the host atoms. The effect of quantum size effects induced by similar or different parameters on the transmittance properties of chalcogenides thin films has been reported by other research groups independent of the deposition technique, in the literature [31-32]..

Fig. 2 show the variation of the absorbance against wavelength plots. The result indicate that the absorbance decreased in the blue region of the electromagnetic spectrum (lower wavelengths) up to the region of the fundamental absorption, and then decreased gradually to minima at the region of lower photon energies (longer wavelengths). In the literature, such observation are common in the absorbance versus wavelength plots for various chalcogenides thin films [30-34]. An important observation in Fig. 2 is that the absorbance were typically lower for the films grown at the higher concentrations, and higher for films doped at concentrations ≤ 0.2 M, and exhibiting maximum values for the as-deposited film.

Fig. 3 show the plots of $(\alpha h v)^2$ vs hv. The optical absorption coefficient α, was calculated using the formula contained in the literature [35-38] as;

$$\alpha = \frac{1}{d} \ln\left(\frac{100}{T\,\%}\right) \tag{1}$$

In equation (1), α retains its meaning, d is the film thickness (in nm for this study), and T is the transmittance in percentage. The optical absorption coefficients data were used to evaluate the energy band gap according to the relation contained in the literature [38-39] as;

$$(\alpha h v) = B(h v - E_g)^n \tag{2}$$

As shown in equation (2), α retains its meaning, h is the Planck's constant, v is the frequency of the electromagnetic radiation, B is an energy independent constant, but generally depend on the refractive index and the effective masses of
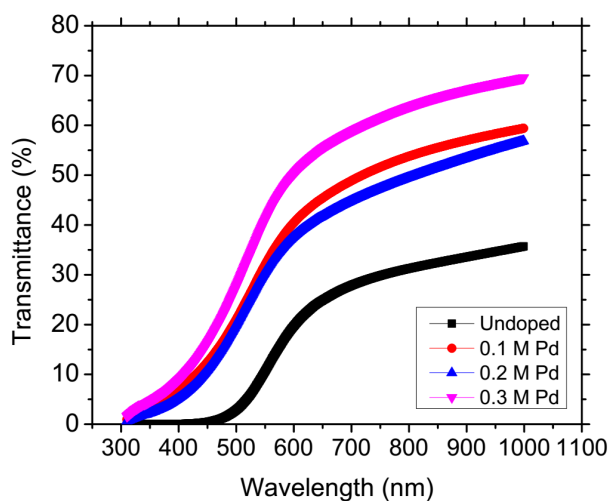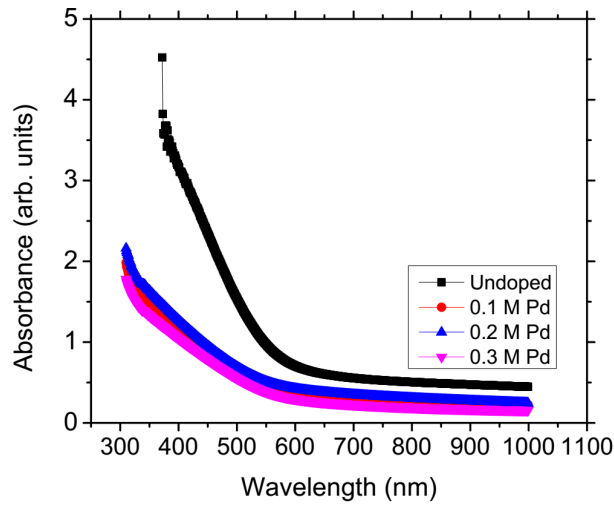

Fig. 1. Transmittance vs wavelength plots
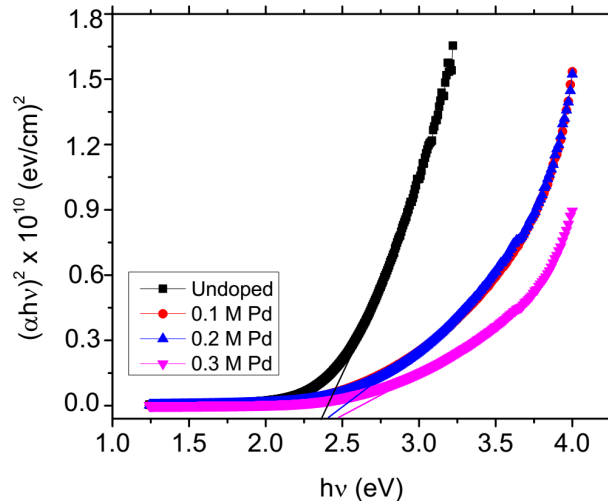
Fig. 2 Absorbance vs wavelength plots

Fig.3. Plots of (αhv)² vs hv.

the hole and electron respectively [38], Eg is the energy band gap, and n is an index that determines the nature of the transition exhibited by the materials under investigation. In direct transition, it is universally accepted that n = 0.5. A close look on Fig.3, clearly reveals that the transition are all direct with values in the range 2.30 eV to 2.48 eV. The values are within the range reported by other research groups [30-32], and also confirms that the films could be used in different optoelectronic applications especially in solar cell devices, lasers, and light emitting diodes (LED). It also explores the possibilty of fabricating Sb₂S₃-based homojunction solar cell devices with improved efficiencies.

Fig. 4 shows the variation of the extinction coefficient with photon energy. The extinction coefficient was calculated using the relation contained in the literature [7, 16, 18-19, 36, 39] as;

$$k = \frac{\alpha\lambda}{4\pi} \qquad (3)$$

In equation (3), α retains its meaning, λ is the wavelength (300 nm to 1000 nm), and π is a constant. The extinction coefficients increased gradually down to the region of the fundamental absorption and then increased. The plots for the as-deposited layers were also higher compared to that of the doped layers. As shown in Fig. 4,
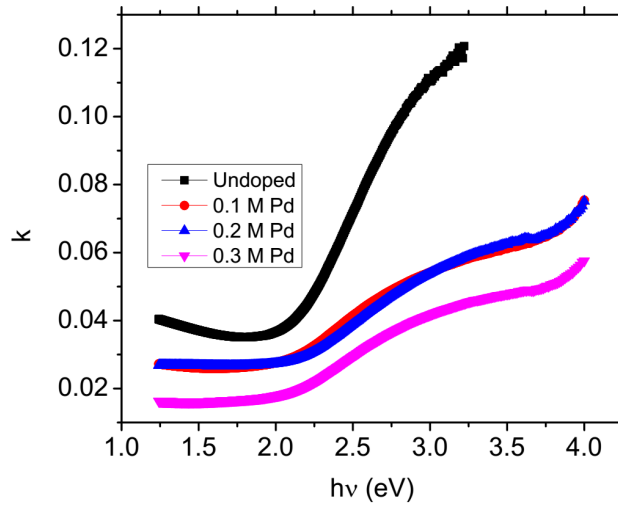
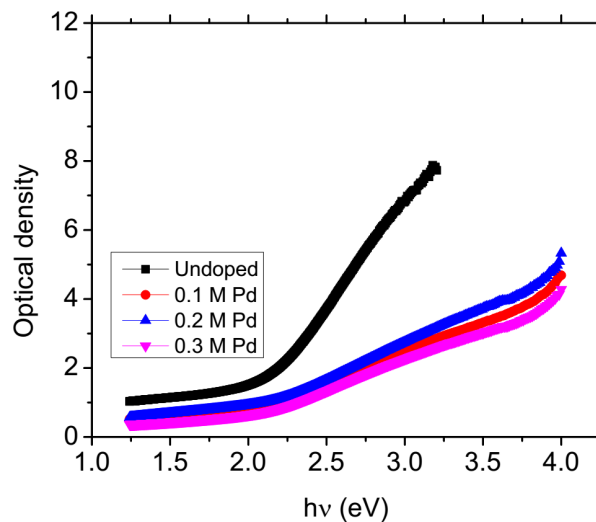Fig. 4. Plots of extinction coefficient k, vs photon energy.

Fig. 5. Plots of optical density vs photon energy.

it was also observed that the films grown at concentrations ≥ 0.3 M exhibited lower values of the extinction coefficient compared to the films doped with palladium impurites of concentrations ≤ 0.2 M. Such behaviour is typical of most thin films including the chalcogenides family. This behaviour observed in Fig. (4) is in agreement with the reports of other research groups [18-19, 39-40] in the literature.

Fig. 5 show the variation of the optical density with the photon energy for the as-deposited antimony sulphide thin films, and at the various concentrations of the dopants investigated in the study. The optical density was calculated using the relation [40];

$$Optical \quad density \quad = \quad \alpha d \qquad (4)$$

In equation (4), α retains its meaning and d is the film thickness. The optical density were typically in the range 1.2 to 8.3.

Fig. 6. show the change imposed on the variation of the energy band gap and film thickness with the different concentrations of the dopants. The values the energy band gap was highest for the as-grown layer (i.e zero palladium impurity), and then increased gradually with an increase in the concentration of the palladium impurities. The film thicknesses also exhibited similar corresponding increase with increase of the dopants.
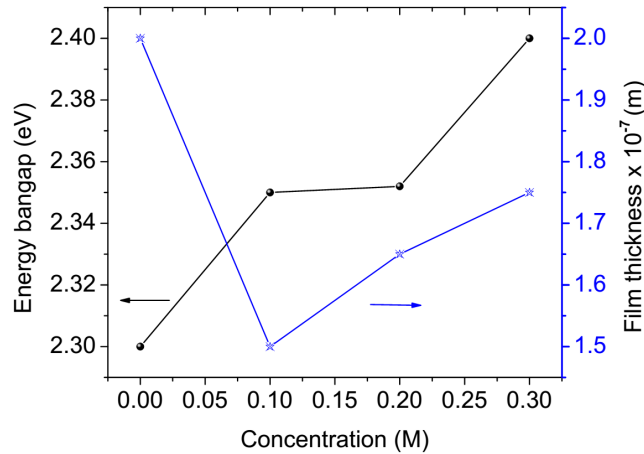
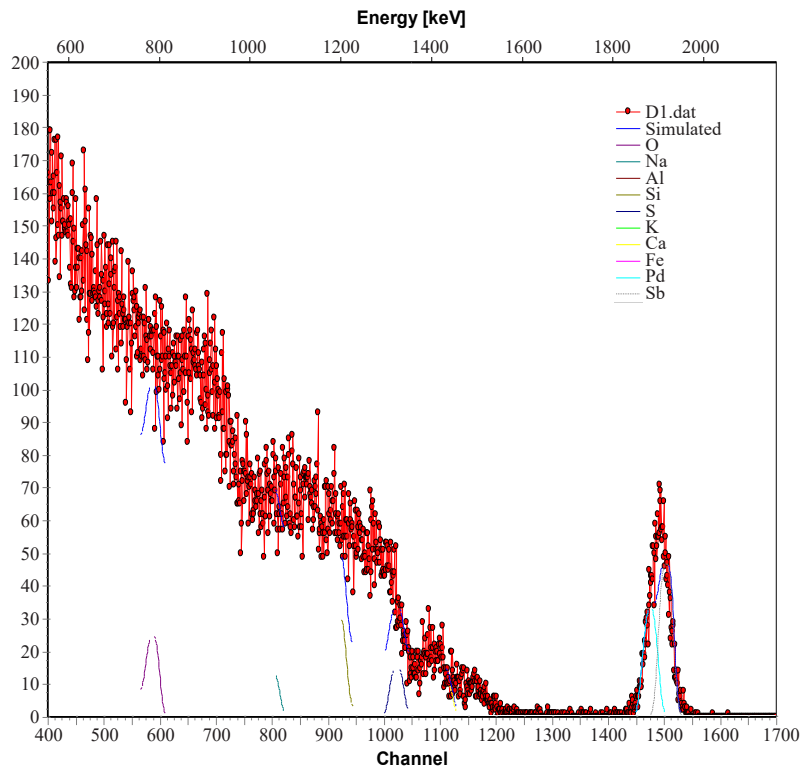Fig. 6. Plots of film thickness and energy band gap with concentration

Fig. 7. RBS plot of the 0.3 M doped layer after annealing

Figs. 7. show a typical RBS plots, indicating the influence of the dopant impurities on the composition of the layers. The results show that the post-deposition heat treatments of the layers influenced the composition in that the percentage of oxygen was relatively high in all the annealed cases. It is possible that this increased oxidation during the annealing process also contributes significantly to the shift of the energy band gap toward higher values.

Fig. 8. gives the X-ray diffractograms of the layers. The result from the X-ray diffractometry indicates that the layers crystallised in stibnite orthorombic crystal structure, consistent with the International Centre for Diffraction Data (ICDD) Powder Diffraction File- PDF:001-0538. The results
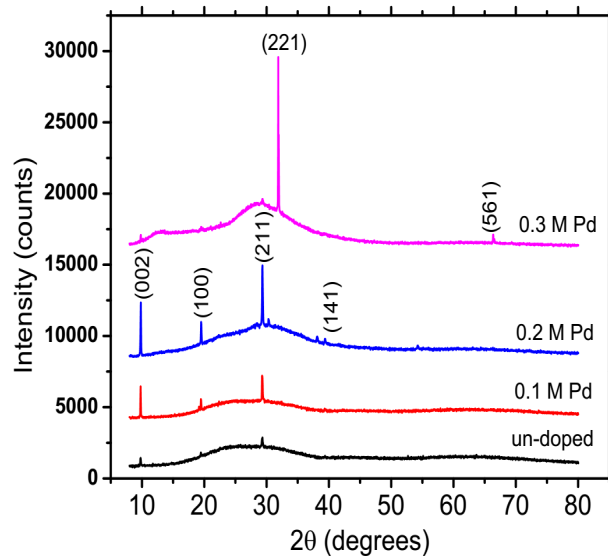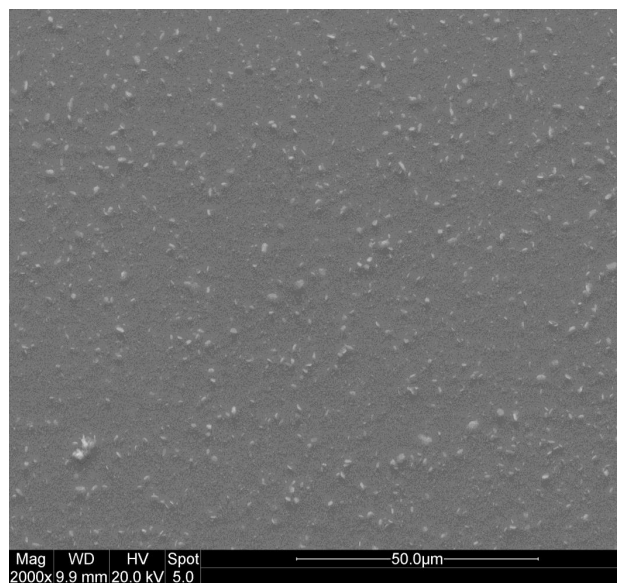
Fig. 8. X-ray diffractograms of the layers

Fig.9. SEM micrograph of the un-doped layer

show diffraction peaks in all the layers, indicating that they are all polycrystalline. However the effect of the concentrations of the palladium impurities on the X-ray diffractograms are clearly pronounced especially with respect to the degree of texturing. At the higher concentrations of the dopants, the diffraction peaks belonging to (002), (100) and (211) were increasing consistently with an increase in concentrations of the palladium impurities. The plots (Fig. 8) also show that at concentration of 0.3 M, there was a suppresion of the other diffraction peaks, with the (221) peaks appearing as the most prominent diffraction peaks. Such variation of the diffraction peaks caused by change in concentration and/or other deposition variables have been widely reported by other authors for similar/related chlacogenides in the literature [41-50].

Fig. 9 shows the SEM micrograph of the un-doped layer while Fig. 10 shows the SEM micrograph of the layer that was doped with 0.3 M of the palladium impurities. Physical observation
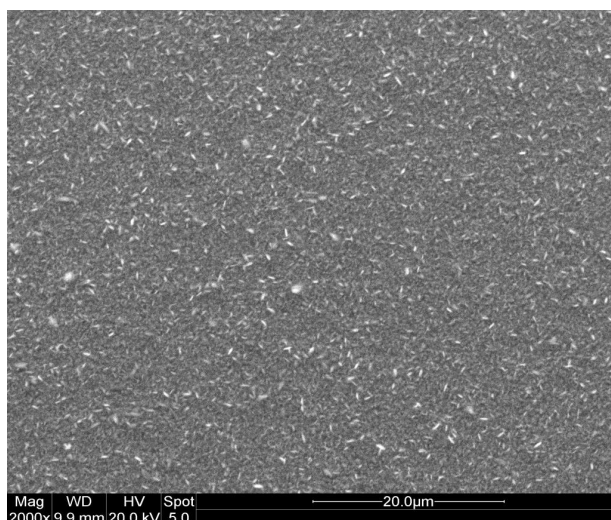
242

Fig.10. SEM micrograph of 0.3 M doped layer

of the micrographs clearly indicate that the increase in the concentration of dopants generally increased the crystallites. The grains show seed-like structures and were uniformly packed. Other authors have observed similar findings in the literature [41-50].

CONCLUSIONS

The influence of palladium impurities at different concentrations on the compositional and optical properties of chemically deposited antimony sulphide thin films is reported. The results show that the presence of the dopants modified the optical properties significantly. In particular, the transmittances of the doped layers were higher compared to the transmittances of the as-deposited films. The energy band gap were found to be direct in both cases, with values in the range 2.30 eV to 2.38 eV. The extinction coefficient were typically lower for the palladium doped layers. The values of the energy band gap strongly indicate that the films could be used in different device designs including optoelectronic applications especially as absorber layers in solar cell devices.

ACKNOWLEDGEMENTS

CONFLICT OF INTEREST

The authors declare that there are no conflicts of interest regarding the publication of this manuscript.

REFERENCES

1. Choi YC, Lee DU, Noh JH, Kim EK, Seok SI. Highly Improved Sb$_2$S$_3$ Sensitized-Inorganic–Organic Heterojunction Solar Cells and Quantification of Traps by Deep-Level Transient Spectroscopy. Adv. Funct. Mater. 2014; 24(23):3587-92.

2. Murtaza G, Akhtar M, Malik MA, O'Brien P, Revaprasadu N. Aerosol assisted chemical vapor deposition of Sb$_2$S$_3$ thin films: Environmentally benign solar energy material. Mater. Sci. Semicond. Process. 2015; 40:643-9.

3. Choi YC, Seok SI. Efficient Sb$_2$S$_3$-Sensitized Solar Cells Via Single-Step Deposition of Sb2S3 Using S/Sb-Ratio-Controlled SbCl$_3$-Thiourea Complex Solution. Adv. Funct. Mater. 2015; 25(19):2892-8.

4. Nikolakopoulou A, Raptis D, Dracopoulos V, Sygellou L, Andrikopoulos KS, Lianos P. Study of upscaling possibilities for antimony sulfide solid state sensitized solar cells. J. Power Sources. 2015; 278:404-10.

5. You MS, Lim CS, Kwon DH, Heo JH, Im SH, Chae KJ. Oxide-free Sb$_2$S$_3$ sensitized solar cells fabricated by spin and heat-treatment of Sb (III)(thioacetamide)$_2$ Cl$_3$. Org Electron. 2015; 21:155-9.

6. Pérez-Martínez D, Gonzaga-Sánchez JD, Bray-Sánchez F, Vázquez-García G, Escorcia-García J, Nair MT, Nair PK. Simple solar cells of 3.5% efficiency with antimony sulfide-selenide thin films. Phys. Status Solidi Rapid Res. Lett. 2016;10(5):388-96.

7. Mushtaq S, Ismail B, Zeb MA, Kissinger NS, Zeb A. Low-temperature synthesis and characterization of Sn-doped Sb$_2$S$_3$ thin film for solar cell applications. J. Alloys Compd. 2015;632:723-8.

8. González-Lúa R, Escorcia-García J, Pérez-Martínez D, Nair MT, Campos J, Nair PK. Stable performance of chemically deposited antimony sulfide-lead sulfide thin film solar cells

under concentrated sunlight. ECS J. Solid State Sci. Technol. 2015;4(3):Q9-16.

9. Yang RX, Butler KT, Walsh A. Assessment of Hybrid Organic–Inorganic Antimony Sulfides for Earth-Abundant Photovoltaic Applications. J. Phys. Chem. Lett. 2015;6(24):5009-14.

10. Choi YC, Lee YH, Im SH, Noh JH, Mandal TN, Yang WS, Seok SI. Efficient Inorganic-Organic Heterojunction Solar Cells Employing $Sb_2(S_x/Se_{1-x})$ 3 Graded-Composition Sensitizers. Adv. Energy Mater. 2014;4(7):1301680.

11. Yang RX, Butler KT, Walsh A. Assessment of Hybrid Organic–Inorganic Antimony Sulfides for Earth-Abundant Photovoltaic Applications. J. Phys. Chem. Lett. 2015;6(24):5009-14.

12. Ornelas-Acosta RE, Shaji S, Avellaneda D, Castillo GA, Roy TD, Krishnan B. Thin films of copper antimony sulfide: a photovoltaic absorber material. Mater. Res. Bull. 2015; 61:215-25.

13. Yuan S, Deng H, Dong D, Yang X, Qiao K, Hu C, Song H, Song H, He Z, Tang J. Efficient planar antimony sulfide thin film photovoltaics with large grain and preferential growth. Sol. Energy Mater Sol. Cells. 2016; 157:887-93.

14. Ramos Aquino JA, Rodriguez Vela DL, Shaji S, Avellaneda DA, Krishnan B. Spray pyrolysed thin films of copper antimony sulfide as photovoltaic absorber. Phys. Status Solidi C. 2016; 13(1):24-9.

15. Boughalmi R, Boukhachem A, Kahlaoui M, Maghraoui H, Amlouk M. Physical investigations on Sb2S3 sprayed thin film for optoelectronic applications. Mater. Sci. Semicond. Process. 2014; 26:593-602.

16. Ali N, Ahmed R, ul Haq B, Shaari A, Hussain R, Goumri-Said S. A novel approach for the synthesis of tin antimony sulphide thin films for photovoltaic application. Solar energy. 2015; 113:25-33.

17. Sun RD, Tsuji T. Preparation of antimony sulfide semiconductor nanoparticles by pulsed laser ablation in liquid. Appl. Surf. Sci. 2015; 348:38-44

18. Shaji S, Garcia LV, Loredo SL, Krishnan B, Martinez JA, Roy TD, Avellaneda DA. Antimony sulfide thin films prepared by laser assisted chemical bath deposition. Appl. Surf. Sci. 2017; 393:369-76.

19. Garcia RA, Avendaño CM, Pal M, Delgado FP, Mathews NR. Antimony sulfide (Sb2S3) thin films by pulse electro-deposition: Effect of thermal treatment on structural, optical and electrical properties. Mater. Sci. Semicond. Process. 2016; 44:91-100.

20. Wan L, Ma C, Hu K, Zhou R, Mao X, Pan S, Wong LH, Xu J. Two-stage co-evaporated $CuSbS_2$ thin films for solar cells. J. Alloys Compd. 2016; 680:182-90.

21. Vinayakumar V, Shaji S, Avellaneda D, Roy TD, Castillo GA, Martinez JA, Krishnan B. $CuSbS_2$ thin films by rapid thermal processing of Sb_2S_3-Cu stack layers for photovoltaic application. Sol. Energy Mater Sol. Cells. 2017;164:19-27.

22. Sun P, Yao F, Ban X, Huang N, Sun X. Directly hydrothermal growth of antimony sulfide on conductive substrate as efficient counter electrode for dye-sensitized solar cells. Electrochim. Acta. 2015; 174:127-32.

23. Lakhdar MH, Ouni B, Amlouk M. Thickness effect on the structural and optical constants of stibnite thin films prepared by sulfidation annealing of antimony films. Optik-International Journal for Light and Electron Optics. 2014, 125(10):2295-301.

24. Suriakarthick R, Kumar VN, Shyju TS, Gopalakrishnan R. Effect of substrate temperature on copper antimony sulphide thin films from thermal evaporation. J. Alloys Compd.. 2015; 651:423-33.

25. Hussain A, Ahmed R, Ali N, Butt FK, Shaari A, Shamsuri WW, Khenata R, Prakash D, Verma KD. Post annealing effects on structural, optical and electrical properties of CuSbS2 thin films fabricated by combinatorial thermal evaporation technique. Superlattices Microstruct. 2016; 89:136-44.

26. Huerta-Flores AM, García-Gómez NA, Salomé M, Sánchez EM. Comparative study of Sb_2S_3, Bi_2S_3 and In_2S_3 thin film deposition on TiO_2 by successive ionic layer adsorption and reaction (SILAR) method. Mater. Sci. Semicond. Process. 2015; 37:235-40.

27. Kozytskiy AV, Stroyuk OL, Skoryk MA, Dzhagan VM, Kuchmiy SY, Zahn DR. Photochemical formation and photoelectrochemical properties of TiO_2/Sb_2S_3 heterostructures. J. Photochem. Photobiol. A. 2015; 303:8-16.

28. Chang YC, Suriyawong N, Aragaw BA, Shi JB, Chen P, Lee MW. Lead antimony sulfide (Pb5Sb8S17) solid-state quantum dot-sensitized solar cells with an efficiency of over 4%. J. Power Sources. 2016; 312:86-92.

29. Choi YC, Yeom EJ, Ahn TK, Seok SI. $CuSbS_2$-Sensitized Inorganic–Organic Heterojunction Solar Cells Fabricated Using a Metal–Thiourea Complex Solution. Angew chem int edit. 2015; 54(13):4005-9.

30. Shaji S, Arato A, O'Brien JJ, Liu J, Castillo GA, Palma MM, Roy TD, Krishnan B. Chemically deposited Sb_2S_3 thin films for optical recording. J. Phys. D: Appl. Phy D. 2010; 43(7):075404.

31. Lakhdar MH, Ouni B, Amlouk M. Dielectric relaxation, modulus behavior and conduction mechanism in Sb_2S_3 thin films. Mater. Sci. Semicond. Process. 2014; 19:32-9.

32. Han Q, Yuan Y, Liu X, Wu X, Bei F, Wang X, Xu K. Room-temperature synthesis of self-assembled Sb_2S_3 films and nanorings via a two-phase approach. Langmuir. 2012; 28(17):6726-30.

33. DeAngelis AD, Kemp KC, Gaillard N, Kim KS. Antimony (III) sulfide thin films as a photoanode material in photocatalytic water splitting. ACS Appl. Mater. Interfaces. 2016; 8(13):8445-51.

34. Bansal N, O'Mahony FT, Lutz T, Haque SA. Solution Processed Polymer–Inorganic Semiconductor Solar Cells Employing Sb_2S_3 as a Light Harvesting and Electron Transporting

Material. Adv. Energy Mater. 2013; 3(8):986-90.

35. M.D. Jeroh, D.N. Okoli, Optical and structural properties of amorphous antimony sulphide thin films: Effect of dip time. Adv. Appl. Sci. Res. 2012;3(2):793-800.

36. Tanuševski A, Poelman D. Optical and photoconductive properties of SnS thin films prepared by electron beam evaporation. Sol. Energy Mater Sol. Cells. 2003;80(3): 297-303.

37. Tanusevski A. Optical and photoelectric properties of SnS thin films prepared by chemical bath deposition. Semicond. Sci. Technol. 2003;18(6): 501.

38. Pankove J.I. Optical Processes in Semiconductors, Prentice-Hall, Englewood Cliffs, New Jersey, 1971.

39. Ismail B, Mushtaq S. Khan RA, Khan AM, Zeb A, Khan AR. Enhanced grain growth and improved optical properties of the Sn doped thin films of Sb2S3 orthorhombic phase. Optik-International Journal for Light and Electron Optics. 2014;125(21): 6418-6421.

40. Cifuentes C, Botero M, Romero E, Calderon C, Gordillo G. Optical and structural studies on SnS films grown by co-evaporation. Braz. J. Phys. 2006;36(3B): 1046-1049.

41. Zinatloo-Ajabshir S, Mortazavi-Derazkola S, Salavati-Niasari M. Sono-synthesis and characterization of Ho 2O3 nanostructures via a new precipitation way for photocatalytic degradation improvement of erythrosine. Int. J. Hydrogen Energy. 2017; 42(22):15178-88.

42. Zinatloo-Ajabshir S, Salavati-Niasari M. Nanocrystalline Pr 6 O 11: synthesis, characterization, optical and photocatalytic properties. New J. Chem. 2015; 39(5):3948-55.

43. Zinatloo-Ajabshir S, Salavati-Niasari M, Zinatloo-Ajabshir Z. Facile size-controlled preparation of highly photocatalytically active praseodymium zirconate nanostructures for degradation and removal of organic pollutants. Sep. Purif. Technol. 2017;177:110-20.

44. Razi F, Zinatloo-Ajabshir S, Salavati-Niasari M. Preparation and characterization of HgI$_2$ nanostructures via a new facile route. Mater. Lett. 2017; 193:9-12.

45. Zinatloo-Ajabshir S, Morassaei MS, Salavati-Niasari M. Facile fabrication of Dy$_2$Sn$_2$O$_7$-SnO$_2$ nanocomposites as an effective photocatalyst for degradation and removal of organic contaminants. J. Colloid Interface Sci. 2017; 497:298-308.

46. Zinatloo-Ajabshir S, Salavati-Niasari M. Preparation of nanocrystalline cubic ZrO$_2$ with different shapes via a simple precipitation approach. J. Mater. Sci. Mater. Electron. 2016; 27(4):3918-28.

47. Nwofe PA, Reddy KR, Miles RW. Type conversion of p-SnS to n-SnS using a SnCl$_4$/CH$_3$OH heat treatment. IEEE 39th Photovoltaic Specialists Conference (PVSC) 2013; 14115963:2518-2523

48. Agbo PE, Nwofe PA. Structural and Optical Properties of Sulphurised Ag$_2$S Thin Films. IJTFST. 2015;4(1):9-12.

49. Morassaei MS, Zinatloo-Ajabshir S, Salavati-Niasari M. Simple salt-assisted combustion synthesis of Nd$_2$Sn$_2$O$_7$–SnO$_2$ nanocomposites with different amino acids as fuel: an efficient photocatalyst for the degradation of methyl orange dye. J. Mater. Sci. Mater. Electron. 2016; 27(11):11698-706.

50. Beshkar F, Zinatloo-Ajabshir S, Bagheri S, Salavati-Niasari M. Novel preparation of highly photocatalytically active copper chromite nanostructured material via a simple hydrothermal route. PLoS One. 2017 ;12(6):e0158549.